NADH Regeneration: A Case Study of Pt-catalyzed NAD^+ Reduction with H_2

Tony Saba,[a,#] Jianwei Li,[a,b,#] Joseph W.H. Burnett,[a] Russell F. Howe,[c] Panagiotis N. Kechagiopoulos,[a] and Xiaodong Wang[a,b,*]

[a]Chemical and Materials Engineering, School of Engineering, University of Aberdeen, Aberdeen AB24 3UE, Scotland, United Kingdom

[b]Chemical Engineering, Department of Engineering, Lancaster University, Lancaster LA1 4YW, United Kingdom

[c]Chemistry Department, University of Aberdeen, Aberdeen AB24 3UE, United Kingdom

*Corresponding Author E-mail:

xiaodong.wang@lancaster.ac.uk

[#]These authors contributed equally

Abstract:

This study shows the importance of resolving catalytic performance in the regeneration of the reduced form of nicotinamide adenine dinucleotide (NADH) through activity measurements based on NAD^+ conversion and the closure of mass balance *via* by-product quantification. This approach is applied to assess the performance of supported platinum catalysts with varying points of zero charge, utilizing H_2 as a reductant. It was found that Pt/SiO_2, which exhibits a net negative charge under the reaction conditions, outperforms the neutral Pt/C and positively charged Pt/MgO due to the favorable electrostatic attraction between the catalyst surface and positively charged (+1) nicotinamide ring. NMR spectroscopy identifies side-products formed during NAD^+ hydrogenation.

Keywords: cofactor; supported Pt; conversion; selectivity; mass balance; by-product

Oxidoreductases account for one-fourth of all known enzymes and with their exclusive and highly desirable properties (high activity, enantioselectivity and mild operating conditions), they have been used in a wide range of biotransformations, including the synthesis of chemicals and pharmaceuticals, biodegradation and detoxification.[1,2] The majority of oxidoreductases depend on a nicotinamide adenine dinucleotide cofactor in its reduced form, NAD(P)H, or its oxidized form, $NAD(P)^+$, to transfer the required reducing or oxidizing equivalent to the substrate.[3] Despite being prolific cofactors, the high cost and the stoichiometric amounts required make the consumption of these cofactors impractical.[4] This has motivated significant research in recycling NAD(P)H from $NAD(P)^+$ to make the reductive process economically feasible (**Scheme 1**). Over the last 50 years, NAD(P)H regeneration using biocatalytic, chemical, electrochemical, photochemical, homogeneous catalytic and heterogeneous catalytic methods have been investigated.[4,5]

It is noteworthy that the reported regeneration studies have almost exclusively used the yield of NAD(P)H (either validated or unvalidated by enzymatic assays) as a performance indicator.[6-21] It would not be an issue for enzymatic regeneration as enzymes are intrinsically selective meaning the yield is equivalent to conversion. This is, however, not applicable for non-enzymatic regeneration as it has been frequently reported that unselective products (e.g., the enzymatically inactive 1,6-NADH, 1,2-NADH, NAD_2 dimers and cofactor decay products,[17-21] **Scheme 1**) can be formed. In fact, for any other catalytic reaction system, conversion and selectivity are indeed more fundamental and typically discussed. A thorough search of the literature did not unearth any studies reporting experimentally measured $NAD(P)^+$ conversion, except when a validated yield approaches ~100% as convincingly demonstrated by the works of Antonietti (photocatalysis[22]), Fukuzumi (homogeneous catalysis[23]) and Minteer (electrocatalysis[24]). When the yield is lower, as is the case in most studies, relying on the yield of NAD(P)H alone as a performance indicator provides little information and, importantly, discloses no information on mass/carbon balance.

In this work, we have examined, for the first time, the conversion, selectivity and mass balance during the course of NAD^+ reduction reactions for NADH regeneration, employing supported Pt catalysts (Pt/SiO_2, Pt/C and Pt/MgO) and using H_2 as a reducing agent. Different by-products have been characterized with their relative contribution towards the overall NAD^+ conversion also investigated. The results have demonstrated a clear contrast to the analysis obtained from a "yield-only" approach and show fundamentals of the support effect as well as by-product formation that otherwise would have been missed.

The catalysts employed have been fully characterized (see **Figures S1-3** for details), with key results summarized in **Table 1**. Pt/SiO_2 and Pt/MgO exhibit type IV isotherms with a H1 hysteresis loop characteristic of mesoporous materials. Both catalysts possess spherical Pt nanoparticles that are well dispersed with narrow size distributions and mean particle sizes of 2.2 and 2.4 nm, respectively. A commercial Pt/C hydrogenation catalyst was used for comparison purposes. The Pt/C exhibits typical activated carbon characteristics in terms of surface area and porosity, where the Pt particles are also well dispersed on the carrier with a narrow size distribution (1-3 nm) and an average size of 1.6 nm. The point of zero charge (pZC) values of the catalysts were determined by the pH drift method (**Table 1** and **Figure S4**). For Pt/SiO_2, at a pH of 3.0 the surface net charge is zero, meaning neutral hydroxylation of Si (Si-OH). Deprotonation of the surface can occur if the catalyst pZC is lower than the working pH, resulting in a negatively charged surface ($Si\text{-}O^-$). Protonation occurs when the pZC is higher than the working pH, resulting in a positively charged surface ($Si\text{-}OH_2^+$).[25] Referring to **Figure S4**, it can be seen that for Pt/SiO_2 most of the curve lies in the negative region ($\Delta pH < 0$) showing its ability to be negatively charged under biologically relevant conditions that require a pH higher than 3.0. In the case of Pt/C, the pZC was determined to be 7.5 which gives Pt/C a nearly neutral surface at pH 7. Pt/MgO exhibits a high pZC (10.3) which shows that it will be positively charged (due to a protonation process, $Mg\text{-}OH_2^+$) under a reaction pH that is lower than

10.3. The pZC results are in agreement with the literature where the pZCs of SiO_2, activated carbon and MgO were reported between 2.5 and 3.1,[26-28] 7.4 and 7.8,[29,30] and 10 and 12.5,[26] respectively.

The catalytic results are first shown (**Figure S5**) by determining the yield based on all products that exhibit an UV-Vis absorbance at 340 nm ($Y_{340\ nm}$) and applying the absorption coefficient of 1,4-NADH, which is the most frequent yield determination method used in the literature.[6-16] We must note that even though these publications refer to it as a yield of NADH (referring to 1,4-NADH), this cannot hold unless the 340 nm absorbance is solely due to 1,4-NADH, considering that 1,6-NADH and the NAD_2 dimer also exhibit λ_{max} at 345 and ~340 nm, respectively. Importantly it is also well established that non-specific reduction of NAD^+ can produce 1,2-, 1,6-NADH and the dimers. Given this, the results shown in **Figure S5** could not lead to any reliable conclusions on activity/selectivity. We should flag here that the majority of the literature validated only the last experimental sample in terms of its 1,4-NADH concentration, meaning there has been no time-on-stream measurement on how such concentrations were reached. With a recently established method for the quantification of reaction products,[31] we have been able to show, for each time-on-stream experimental point, that the 340 nm absorbance was due to a mixture of 1,4- and 1,6-NADH (individual yields provided in **Figure S5**). There are some variations in terms of $Y_{1,4\text{-NADH}}$ and $Y_{1,6\text{-NADH}}$ over the three catalysts (**Figure S5**), but knowing already they are unselective from the beginning of the regeneration, again no meaningful link can be established between the catalyst characteristics and their performance. Unless a full picture of the reaction profiles (*e.g.*, conversion, selectivity and mass balance) are presented, the conclusions/interpretations argued could potentially be misleading.

With the product selectivity and NAD^+ conversion experimentally determined, the catalytic results are now presented in **Figure 1**. Surprisingly, the mass balance was not closed over the entire course of the reactions, a result that has never been emphasized (or even reported) in the literature. It

appears to be an underlying issue in the development of non-enzymatic regeneration techniques. **Figure 1** shows that for all the catalysts, as the conversion increased with time the selectivity of the unknown (calculated through mass balance closure) decreased then levelled whereas the selectivity of 1,4- and 1,6-NADH increased and stabilized. Pt/SiO_2, Pt/C and Pt/MgO exhibited a conversion of 80.0%, 84.1% and 56.6% in 2 h, respectively, with corresponding initial TOFs of 1600 h^{-1} for Pt/SiO_2, 1123 h^{-1} for Pt/C and 990 h^{-1} for Pt/MgO. The specific activity order matches well with the increasing pZC values (3.0→7.5→10.3, **Figure 1(d)**). This can be attributed to the overall catalyst surface charge, which affects the interactions with the positively charged (+1) nicotinamide ring (where the reaction occurs[32]) via electrostatic forces. At a reaction pH of 7, Pt/SiO_2 has a strong negatively charged surface due to the pZC deprotonation mechanism. This increases the local concentration of nicotinamide ring (+1, **Figure S6**) around the Pt nanoparticles where Pt-H_{ads} species[33,34] are available for hydrogenation, thus enhancing the probability of reactions. On the other hand, at pH 7, both ionizable hydroxyl groups (pK_a = 2.4 and 6.6) on the diphosphate linkage of NAD^+ are deprotonated exhibiting each a charge of -1.[35] This side of the molecule (-2) should exhibit an electrostatic repulsion with the negatively changed surface. Moreover, it is reported that the diphosphate linkage is highly hydrophilic and typically stays in the bulk aqueous buffer solution away from the catalyst surface (**Figure S6**).[32,36] These all support that a negatively charged catalyst surface is favorable for NAD^+ hydrogenation. In the case of the least active Pt/MgO, it has a high pZC of 10.3, corresponding to a positively charged surface that resulted in unfavorable interaction with the nicotinamide ring (+1). Pt/C exhibits a pZC between those of Pt/SiO_2 and Pt/MgO, hence an intermediate activity. The same activity-pZC relationship was also obtained at pH 10 (**Figure S7**), consistent with the above discussions and confirming the surface charge contribution. To this end, Roy and co-workers have recently reported that interactions via electrostatic forces can also influence NADH yield in photocatalytic regeneration.[37] Although the support pZC affected the activity, it had no obvious influence on the selectivity. For instance, at X_{NAD^+} = ~47%, the selectivity of 1,4-NADH were as

follows: 20.2 % for Pt/SiO_2, 25.1 % for Pt/C and 17.8 % for Pt/MgO. It is only through the conversion and mass balance examinations that these observations were obtained. The present results highlight the importance of carefully validating the mass balance and the respective contributions to the 340 nm absorbance prior to claiming any selectivity/yield values, and, hence, arriving at mechanistic assumptions.

In order to shed some light on the unknown product, further experiments on the stability of 1,4-NADH and NAD^+ under various conditions have been conducted. When no catalyst was used, almost 20% of the initial 1,4-NADH was consumed by self-decay in 180 min regardless of the nature of the gas (**Figure 2(a)**), consistent with first order decay kinetics as reported previously.[20,38] 1,4-NADH undergoes an acid-catalyzed hydration reaction to form the primary decay product, 6-hydroxytetrahydropyridine adenine dinucleotide (UV-vis at 290-300 nm).[39] On the other hand, **Figure 2(b)** shows the stability of NAD^+ after 180 min in the presence of N_2 and Pt/C as a representative catalyst. The results of the enzymatic kit (measuring the total concentration of 1,4-NADH and NAD^+)[31] as well as the UV-scans (inset of **Figure 2(b)**) also prove that NAD^+ stays intact throughout time. However, it was interesting to see that in the case of 1,4-NADH when H_2 and Pt/C were used, the rate of concentration decrease was higher with a loss of 65.4% after 180 min, suggesting enhanced decay due to the Pt catalyst which provides protons.[33,34] The results of the enzymatic kit match the actual concentration of 1,4-NADH indicating that 1,4-NADH is the only enzymatically active species present in the reaction medium (*i.e.*, no tautomerization or NAD^+ formation). The results of the UV-scans (see inset of **Figure 2(a)**) conducted at 180 min of each reaction prove the formation of an enzymatically inactive product with absorbance around 290-300 nm. These results demonstrate that once formed, 1,4-NADH may be subject to enhanced decay by the catalyst in the reaction medium and conditions, in line with the following ^1H NMR analysis.

The ^{1}H NMR results obtained from the reduction of NAD^{+} (using Pt/C as a representative catalyst) are shown in **Figure 3**. Singlets are single peaks assigned to hydrogen atoms that do not have any surrounding or neighbor hydrogen. For NAD^{+} (**Figure 3(a)**), the singlet located at around 9.20 ppm is characteristic of the hydrogen H-2' of the nicotinamide moiety.[40] The other two singlets located between 8 and 8.5 ppm are attributed to the hydrogen atoms of the adenine ring.[40,41] In the case of a freshly prepared 1,4-NADH solution (**Figure 3(b)**), the singlet at 6.85 ppm is attributed to the H-2 of the nicotinamide ring,[42] whereas the other two singlets between 8 and 8.5 ppm are characteristic of the adenine ring (in the R group, **Figure S6**).[41] The ^{1}H NMR results of the products at 2 h (**Figure 3(c)**) shows a combination of both NAD^{+} and 1,4-NADH. However, two new singlets appear at 7.01 and 7.13 ppm, characteristics of the by-products formed during regeneration (as evident over all three Pt catalysts, see also **Figure S8**). Knowing that 1,4-NADH can self-decay with time (**Figure 2(a)**),[38,43] a 1,4-NADH sample was left for decay and subsequently ^{1}H NMR spectra of the products were collected (**Figure 3(d)**). The 1,4-NADH decay product appears through a singlet at 7.13 ppm which matches one of the peaks in the NADH regeneration products. The other signal should be due to 1,6-NADH as one of our confirmed products, exhibiting a peak at 7.01 ppm. In order to establish this, we have synthesized a mixture of 1,6- and 1,4-NADH based on borohydride NAD^{+} reduction.[31] The two isomers exhibit NMR peaks at 7.02 and 6.86, respectively (**Figure 3(e)**), in good agreement with our reaction profile confirming the generation of 1,6-NADH. **Figure 2(c)** summarizes the possible NADH regeneration pathways over these Pt catalysts under our reaction conditions. The (catalyzed) decay of 1,4-NADH has often been neglected with prolonged reaction time (*e.g.*, 13h and 21 h) in the literature and if the produced NADH isomers are not enzymatically validated, 1,6-NADH would have been missed. Although not detected in our system, we want to flag the potential formation of 1,2-NADH and/or its decay product. In a nonspecific NAD^{+} reduction system (like borohydride reduction[31] but possibly in other electron transfer processes), 1,2-NADH can be formed but quickly decay in the medium (*e.g.*, a pH 7 phosphate buffer),[31] as evident by the 6.63 ppm peak

in **Figure 3(e)**. Given the "yield-only" approach prevailing in the literature, the NMR profiles should also be examined in detail.

In summary, the examination of conversion, selectivity and mass balance in NADH regeneration is proven critical and can provide reliable performance indicators (*e.g.*, TOF based on NAD^+ consumption). Accordingly, it is shown that an overall negatively charged catalyst surface (*i.e.*, reaction pH higher than pZC) favored the catalytic activity in NADH regeneration while a positively charged surface inhibited the performance. The electrostatic attraction between the catalyst surface (at pH 7, Pt/SiO_2 (negative) > Pt/C (~neutral) > Pt/MgO (positive)) and the positively charged nicotinamide ring (+1) of the NAD^+ molecules increases the local concentration of the nicotinamide ring around Pt and hence the potency of the hydrogenation reaction. In addition to the formation of 1,6-NADH, a Pt enhanced 1,4-NADH decay reaction was also evident. We hope that these results may urge future scrutiny on conversion, selectivity and mass balance closure in non-enzymatic NADH regeneration systems prior to publishing the data.

Supporting Information

The Supporting Information is available free of charge at …

Experimental, results and discussion, figures and references.

ACKNOWLEDGMENTS

This work was supported by The Royal Society (ICA\R1\180317).

REFERENCES

(1) Martínez, A. T.; Ruiz-Dueñas, F. J.; Camarero, S.; Serrano, A.; Linde, D.; Lund, H.; Vind, J.; Tovborg, M.; Herold-Majumdar, O. M.; Hofrichter, M.; Liers C.; Ullrich R.; Scheibner K.; Sannia G.; Piscitelli A.; Pezzella C.; Sener M. E.; Kılıç S.; van Berkel W. J. H.; Guallar V.; Lucas M. F.; Zuhse R.; Ludwig R.; Hollmann F.; Fernández-Fueyo E.; Record E.; Faulds C. B.; Tortajada M.; Winckelmann I.; Rasmussen J. A.; Gelo-Pujic M.; Gutiérrez A.; Del Río J. C.;

Rencoret J.; Alcalde M. Oxidoreductases on Their Way to Industrial Biotransformations. *Biotechnol. Adv.* **2017,** *35* (6), 815-831.

(2) Sellés Vidal, L.; Kelly, C. L.; Mordaka, P. M.; Heap, J. T. Review of NAD(P)H-dependent Oxidoreductases: Properties, Engineering and Application. *BBA-Proteins Proteom.* **2018,** *1866* (2), 327-347.

(3) Cahn, J. K. B.; Werlang, C. A.; Baumschlager, A.; Brinkmann-Chen, S.; Mayo, S. L.; Arnold, F. H. A General Tool for Engineering the NAD/NADP Cofactor Preference of Oxidoreductases. *ACS Synth. Biol.* **2017,** *6* (2), 326-333.

(4) Wang, X.; Saba, T.; Yiu, H. H. P.; Howe, R. F.; Anderson, J. A.; Shi, J. Cofactor NAD(P)H Regeneration Inspired by Heterogeneous Pathways. *Chem* **2017,** *2* (5), 621-654.

(5) Wu, H.; Tian, C.; Song, X.; Liu, C.; Yang, D.; Jiang, Z. Methods for the Regeneration of Nicotinamide Coenzymes. *Green Chem.* **2013,** *15* (7), 1773-1789.

(6) Zhang, L.; Vilà, N.; Kohring, G.-W.; Walcarius, A.; Etienne, M. Covalent Immobilization of (2,2'-Bipyridyl) (Pentamethylcyclopentadienyl)-Rhodium Complex on a Porous Carbon Electrode for Efficient Electrocatalytic NADH Regeneration. *ACS Catal.* **2017,** *7* (7), 4386-4394.

(7) Ganesan, V.; Sivanesan, D.; Yoon, S. Correlation between the Structure and Catalytic Activity of [Cp*Rh(Substituted Bipyridine)] Complexes for NADH Regeneration. *Inorg. Chem.* **2017,** *56* (3), 1366-1374.

(8) Kim, S.; Lee, G. Y.; Baeg, J.-O.; Kim, Y.; Kim, S.-J.; Kim, J. Visible-Light-Driven Photoproduction of Hydrogen Using Rhodium Catalysts and Platinum Nanoparticles with Formate. *J. Phys. Chem. C* **2014,** *118* (45), 25844-25852.

(9) Huang, X.; Liu, J.; Yang, Q.; Liu, Y.; Zhu, Y.; Li, T.; Tsang, Y. H.; Zhang, X. Microfluidic Chip-based One-step Fabrication of An Artificial Photosystem I for Photocatalytic Cofactor Regeneration. *RSC Adv.* **2016,** *6* (104), 101974-101980.

(10) Ji, X.; Liu, C.; Wang, J.; Su, Z.; Ma, G.; Zhang, S. Integration of Functionalized Two-dimensional TaS_2 Nanosheets and An Electron Mediator for More Efficient Biocatalyzed Artificial Photosynthesis. *J. Mater. Chem. A* **2017,** *5* (11), 5511-5522.

(11) Yang, D.; Zou, H.; Wu, Y.; Shi, J.; Zhang, S.; Wang, X.; Han, P.; Tong, Z.; Jiang, Z. Constructing Quantum Dots@Flake Graphitic Carbon Nitride Isotype Heterojunctions for Enhanced Visible-Light-Driven NADH Regeneration and Enzymatic Hydrogenation. *Ind. Eng. Chem. Res.* **2017,** *56* (21), 6247-6255.

(12) Kuk, S. K.; Singh, R. K.; Nam, D. H.; Singh, R.; Lee, J.-K.; Park, C. B. Photoelectrochemical Reduction of Carbon Dioxide to Methanol through a Highly Efficient Enzyme Cascade. *Angew. Chem. Int. Ed.* **2017,** *56* (14), 3827-3832.

(13) Nam, D. H.; Kuk, S. K.; Choe, H.; Lee, S.; Ko, J. W.; Son, E. J.; Choi, E.-G.; Kim, Y. H.; Park, C. B. Enzymatic Photosynthesis of Formate from Carbon Dioxide Coupled with Highly Efficient Photoelectrochemical Regeneration of Nicotinamide Cofactors. *Green Chem.* **2016,** *18* (22), 5989-5993.

(14) Wang, S.; Li, M.; Patil, A. J.; Sun, S.; Tian, L.; Zhang, D.; Cao, M.; Mann, S. Design and Construction of Artificial Photoresponsive Protocells Capable of Converting Day Light to Chemical Energy. *J. Mater. Chem. A* **2017,** *5* (47), 24612-24616.

(15) Ma, B.; Sun, S.; He, H.; Lv, R.; Deng, J.; Huo, T.; Zhao, Y.; Yu, H.; Zhou, L. An Efficient Metal-Free Photocatalytic System with Enhanced Activity for NADH Regeneration. *Ind. Eng. Chem. Res.* **2019,** *58* (51), 23567-23573.

(16) Tarnowicz-Staniak, N.; Vázquez-Díaz, S.; Pavlov, V.; Matczyszyn, K.; Grzelczak, M. Cellulose as an Inert Scaffold in Plasmon-Assisted Photoregeneration of Cofactor Molecules. *ACS Appl. Mater. Interfaces* **2020,** *12* (17), 19377-19383.

(17) Ali, I.; Khan, T.; Omanovic, S. Direct Electrochemical Regeneration of the Cofactor NADH on Bare Ti, Ni, Co and Cd Electrodes: The Influence of Electrode Potential and Electrode Material. *J. Mol. Catal. A: Chem.* **2014,** *387*, 86-91.

(18) Stufano, P.; Paris, A. R.; Bocarsly, A. Photoelectrochemical NADH Regeneration using Pt-Modified p-GaAs Semiconductor Electrodes. *ChemElectroChem* **2017,** *4* (5), 1066-1073.

(19) Beaupre, B. A.; Hoag, M. R.; Roman, J.; Försterling, F. H.; Moran, G. R. Metabolic Function for Human Renalase: Oxidation of Isomeric Forms of β-NAD(P)H that Are Inhibitory to Primary Metabolism. *Biochemistry* **2015,** *54* (3), 795-806.

(20) Li, H.; Worley, K. E.; Calabrese Barton, S. Quantitative Analysis of Bioactive NAD^+ Regenerated by NADH Electro-oxidation. *ACS Catal.* **2012,** *2* (12), 2572-2576.

(21) Wang, X.; Yiu, H. H. P. Heterogeneous Catalysis Mediated Cofactor NADH Regeneration for Enzymatic Reduction. *ACS Catal.* **2016,** *6* (3), 1880-1886.

(22) Liu, J.; Antonietti, M. Bio-inspired NADH Regeneration by Carbon Nitride Photocatalysis using Diatom Templates. *Energy Environ. Sci.* **2013,** *6* (5), 1486-1493.

(23) Maenaka, Y.; Suenobu, T.; Fukuzumi, S. Efficient Catalytic Interconversion between NADH and NAD^+ Accompanied by Generation and Consumption of Hydrogen with a Water-Soluble Iridium Complex at Ambient Pressure and Temperature. *J. Am. Chem. Soc.* **2012,** *134* (1), 367-374.

(24) Yuan, M.; Kummer, M. J.; Milton, R. D.; Quah, T.; Minteer, S. D. Efficient NADH Regeneration by a Redox Polymer-Immobilized Enzymatic System. *ACS Catal.* **2019,** *9* (6), 5486-5495.

(25) Lopez-Ramon, M. V.; Stoeckli, F.; Moreno-Castilla, C.; Carrasco-Marin, F. On the Characterization of Acidic and Basic Surface Sites on Carbons by Various Techniques. *Carbon* **1999,** *37* (8), 1215-1221.

(26) Kosmulski, M. *Surface Charging and Points of Zero Charge*; CRC Press: Boca Raton, 2009.

(27) Velez, J.; Arce, R.; Alburquenque, D.; Gautier, J. L.; Zuñiga, C.; Herrera, F. Simple Steps for Synthesis of Silicon Oxide Mesoporous Materials Used as Template. *J. Chil. Chem. Soc.* **2013,** *58* (4), 1998-2000.

(28) Phanichphant, S.; Nakaruk, A.; Channei, D. Photocatalytic Activity of the Binary Composite CeO_2/SiO_2 for Degradation of Dye. *Appl. Surf. Sci.* **2016,** *387*, 214-220.

(29) Shah, I.; Adnan, R.; Wan Ngah, W. S.; Mohamed, N. Iron Impregnated Activated Carbon as an Efficient Adsorbent for the Removal of Methylene Blue: Regeneration and Kinetics Studies. *PLOS ONE* **2015,** *10* (4), e0122603.

(30) Adam, O. Removal of Resorcinol from Aqueous Solution by Activated Carbon: Isotherms, Thermodynamics and Kinetics. *Am. Chem. Sci. J.* **2016,** *16*, 1-13.

(31) Saba, T.; Burnett, J. W. H.; Li, J.; Kechagiopoulos, P. N.; Wang, X. A Facile Analytical Method for Reliable Selectivity Examination in Cofactor NADH Regeneration. *Chem. Commun.* **2020,** *56* (8), 1231-1234.

(32) Damian, A.; Omanovic, S. Interactive Adsorption Behavior of NAD^+ at a Gold Electrode Surface. *Langmuir* **2007,** *23* (6), 3162-3171.

(33) Song, H.-K.; Lee, S. H.; Won, K.; Park, J. H.; Kim, J. K.; Lee, H.; Moon, S.-J.; Kim, D. K.; Park, C. B. Electrochemical Regeneration of NADH Enhanced by Platinum Nanoparticles. *Angew. Chem. Int. Ed.* **2008,** *47* (9), 1749-1752.

(34) Yang, G.; Akhade, S. A.; Chen, X.; Liu, Y.; Lee, M.-S.; Glezakou, V.-A.; Rousseau, R.; Lercher, J. A. The Nature of Hydrogen Adsorption on Platinum in the Aqueous Phase. *Angew. Chem. Int. Ed.* **2019,** *58* (11), 3527-3532.

(35) Morrison, C. S.; Armiger, W. B.; Dodds, D. R.; Dordick, J. S.; Koffas, M. A. G. Improved Strategies for Electrochemical 1,4-NAD(P)H_2 Regeneration: A New Era of Bioreactors for Industrial Biocatalysis. *Biotechnol. Adv.* **2018,** *36* (1), 120-131.

(36) Wei, H. Z.; van de Ven, T. G. M.; Omanovic, S.; Zeng, Y. W. Adsorption Behavior of Dinucleotides on Bare and Ru-Modified Glassy Carbon Electrode Surfaces. *Langmuir* **2008,** *24* (21), 12375-12384.

(37) Roy, S.; Jain, V.; Kashyap, R. K.; Rao, A.; Pillai, P. P. Electrostatically Driven Multielectron Transfer for the Photocatalytic Regeneration of Nicotinamide Cofactor. *ACS Catal.* **2020,** *10* (10), 5522-5528.

(38) Alivisatos, S. G. A.; Ungar, F.; Abraham, G. J. Spontaneous Reactions of 1,3-Substituted 1,4-Dihydropyridines with Acids in Water at Neutrality. I. Kinetic Analysis and Mechanism of the Reactions of Dihydronicotinamide-Adenine Dinucleotide with Orthophosphates. *Biochemistry* **1965,** *4* (12), 2616-2630.

(39) Johnson, S. L.; Tuazon, P. T. Acid-catalyzed Hydration of Reduced Nicotinamide Adenine Dinucleotide and Its Analogs. *Biochemistry* **1977,** *16* (6), 1175-1183.

(40) de Graaf, R. A.; Behar, K. L. Detection of Cerebral NAD^+ by in vivo ^1H NMR Spectroscopy. *NMR Biomed.* **2014,** *27* (7), 802-809.

(41) Jardetzky, O.; Wade-Jardetzky, N. G. The Conformation of Pyridine Dinucleotides in Solution. *J. Biol. Chem.* **1966,** *241* (1), 85-91.

(42) Meyer, W. L.; Mahler, H. R.; Baker, R. H. Nuclear Magnetic Resonance Spectra and Conformation of 1,4-Dihydropyridines. *Biochim. Biophys. Acta* **1962,** *64* (2), 353-358.

(43) Rover, L.; Fernandes, J. C. B.; Neto, G. d. O.; Kubota, L. T.; Katekawa, E.; Serrano, S. l. H. P. Study of NADH Stability Using Ultraviolet–Visible Spectrophotometric Analysis and Factorial Design. *Anal. Biochem.* **1998,** *260* (1), 50-55.

Table 1

Table 1: Summary of the physicochemical properties of the Pt/SiO_2, Pt/C and Pt/MgO catalysts.

	Pt/SiO_2	Pt/C	Pt/MgO
Pt Loading (%)	0.83	0.93	1.52
BET Surface Area ($m^2\ g^{-1}$)	165	938	86
Pore Volume ($cm^3\ g^{-1}$)	0.9	0.4	0.7
Pore Size (nm)	25.4	5.0	28.3
Particle Size (nm)	2.2	1.6	2.4
pZC (-)	3.0	7.5	10.3

Scheme 1

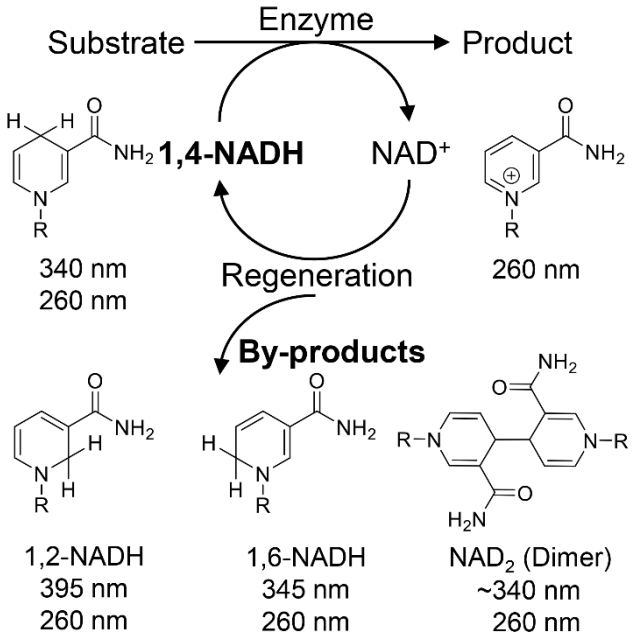

Scheme 1. Schematic representation of biotransformations with *in situ* NADH regeneration that can generate unselective 1,2-NADH, 1,6-NADH and NAD_2 dimer products with their corresponding absorption maxima.

Figure 1

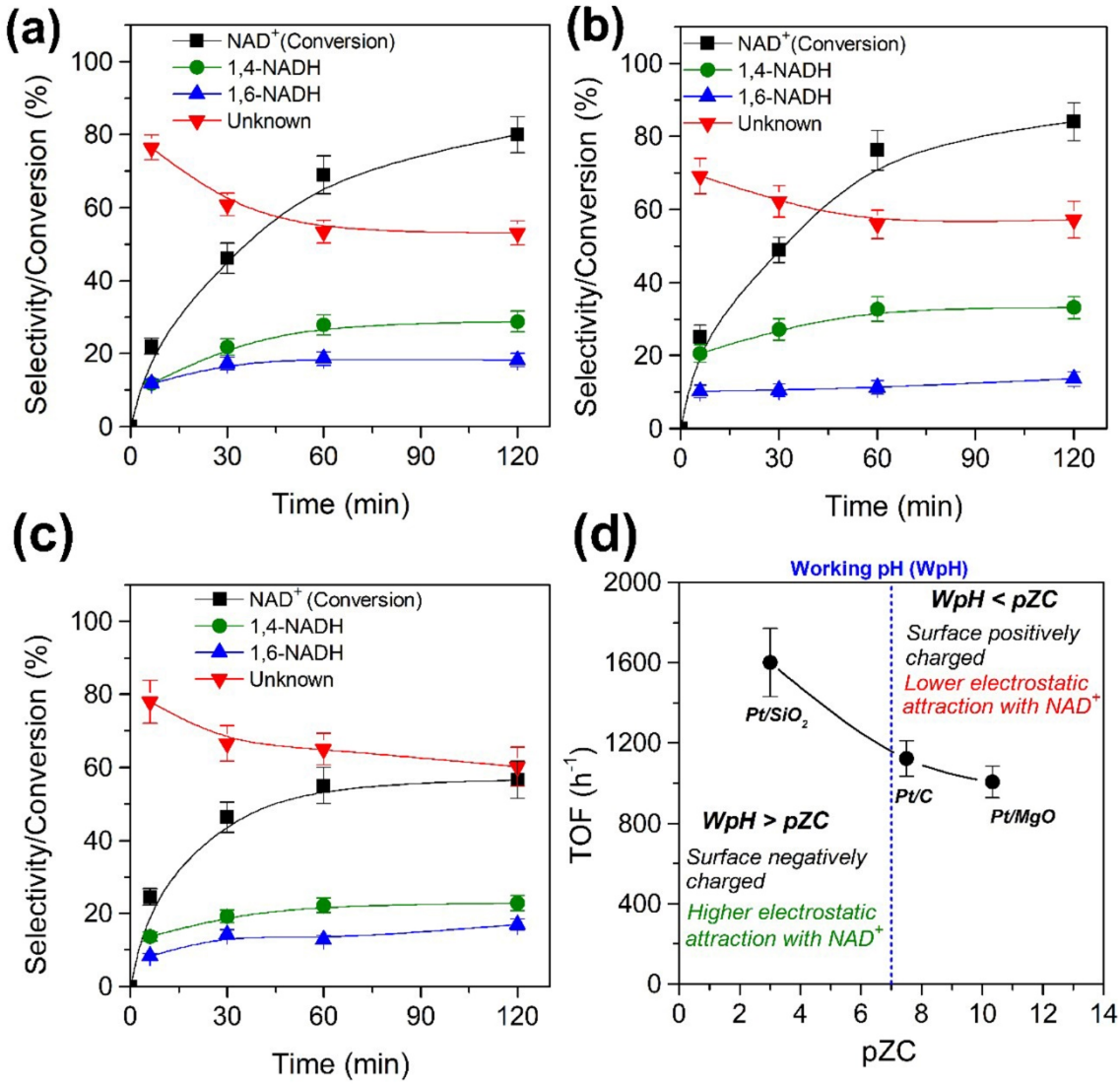

Figure 1. Selectivity and conversion as a function of time in the regeneration of NADH over supported Pt catalysts: Pt/SiO_2 (a), Pt/C (b) and Pt/MgO (c); Effect of catalyst point of zero charge (pZC) on the initial TOF (d). Reaction conditions: $[NAD^+]_0$ = 1.5 mM, 5 mg catalyst, 10 atm H_2, 0.1 M phosphate buffer pH 7, 37 °C, 1200 rpm.

Figure 2

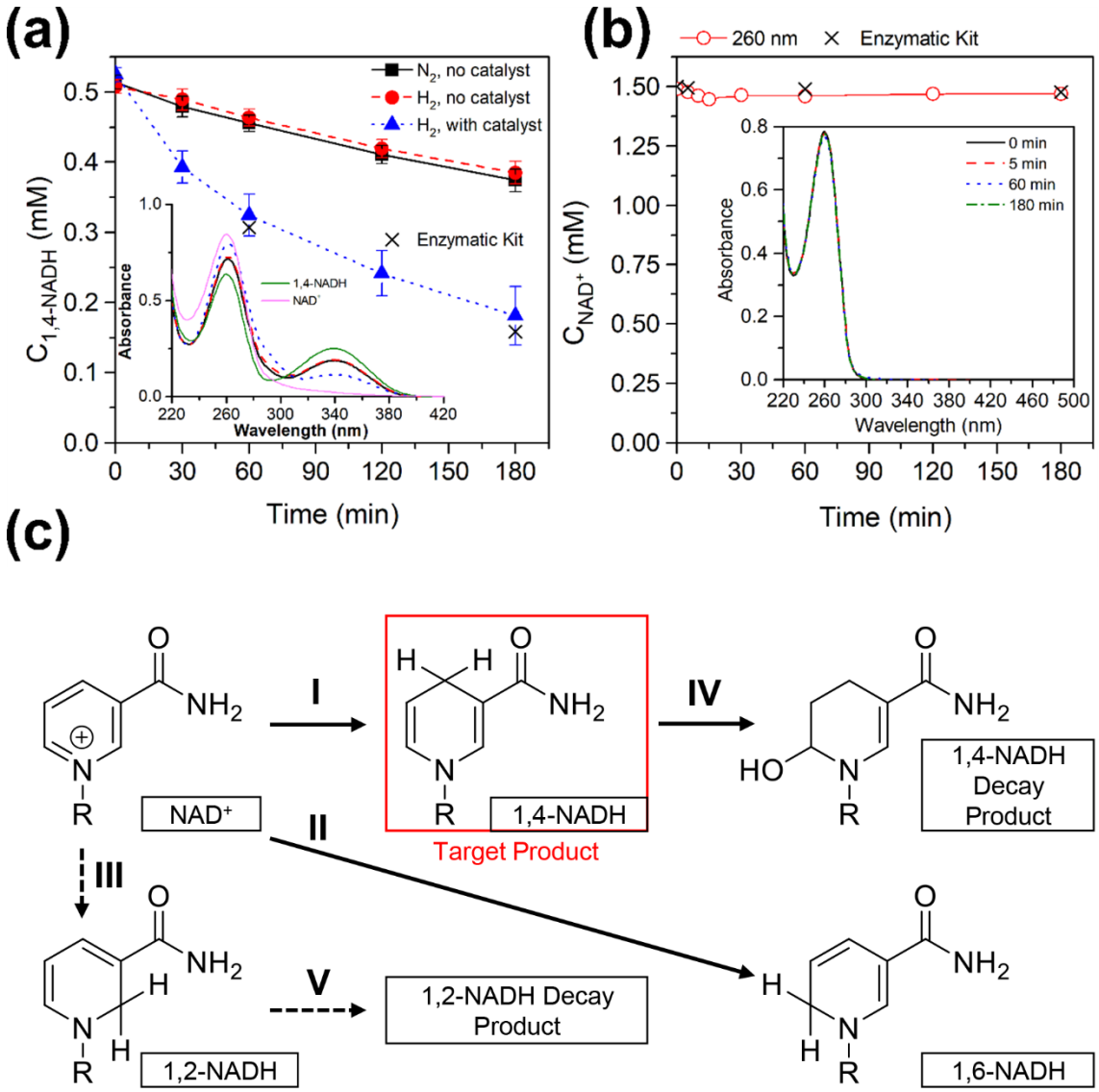

Figure 2. (a) 1,4-NADH stability test ($C_{1,4\text{-NADH}}$ as a function of time) under N_2 and no catalyst, H_2 and no catalyst and H_2 with catalyst (Conditions: $[1,4\text{-NADH}]_0$ = 0.5 mM, 0.1 M phosphate buffer pH 7, 5 mg of Pt/C (if applicable), 37 °C, 10 atm, 1200 rpm); inset: UV-vis absorbance at 180 min with 0.5 mM of NAD^+ and 1,4-NADH as references; (b) NAD^+ stability test (C_{NAD^+} as a function of time) with N_2 and Pt/C catalyst (Conditions: $[NAD^+]_0$ = 1.5 mM, 0.1 M phosphate buffer pH 7, 5 mg of Pt/C, 37 °C, 10 atm, 1200 rpm); inset: UV-vis absorbance in the course of the reaction; (c) Schematic representation of the Pt promoted NADH regeneration pathways.

Figure 3

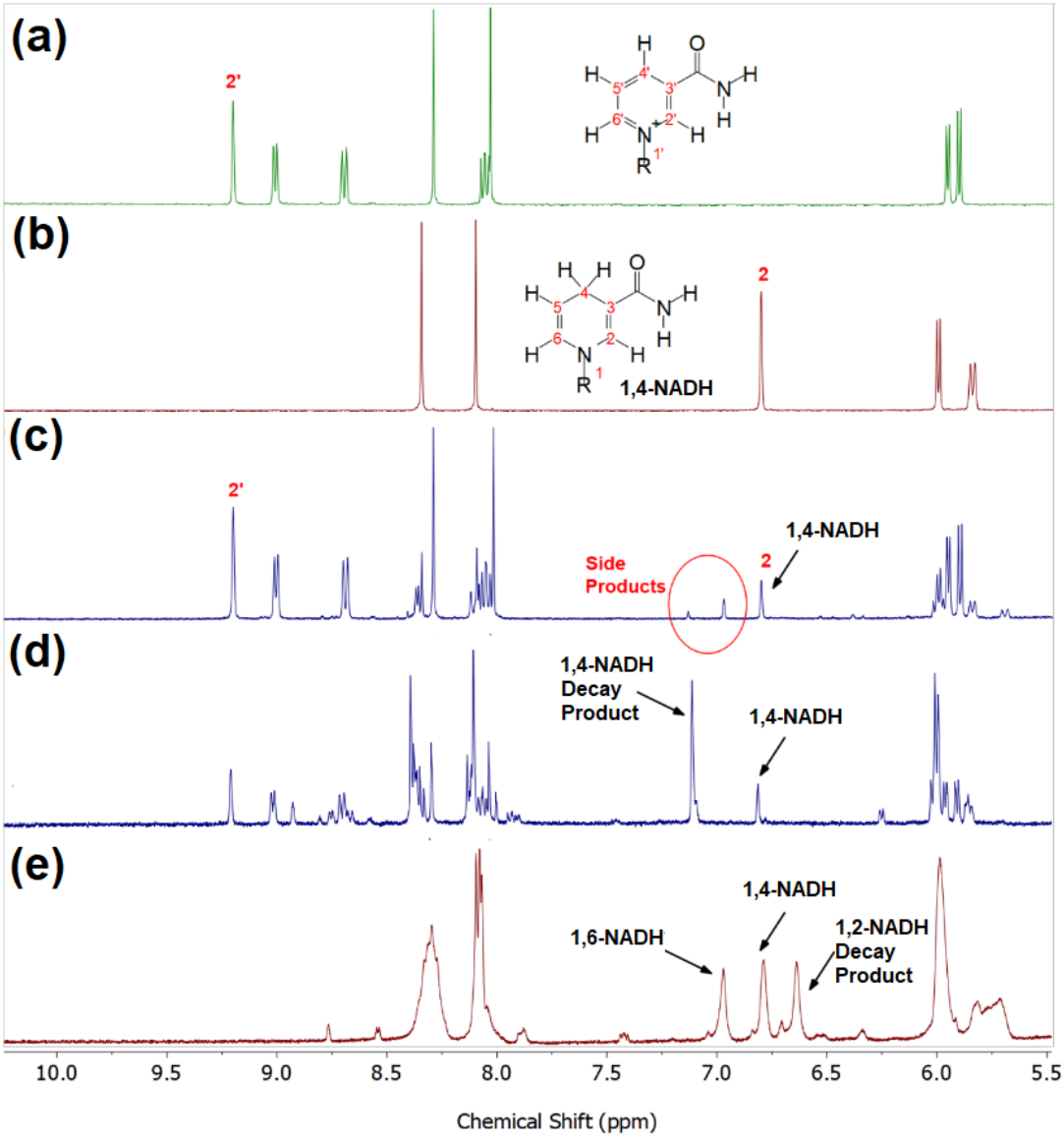

Figure 3. ^{1}H NMR spectra for (a) NAD^+ (C_0 = 6 mM in 0.1 M D_2O phosphate buffer pH 7), (b) 1,4-NADH (C_0 = 6 mM in 0.1 M D_2O phosphate buffer pH 7), (c) Pt/C catalyzed NADH regeneration products ($[NAD^+]_0$ = 6 mM in 0.1 M D_2O phosphate buffer pH 7, 20 mg Pt/C, 37 °C, 10 atm H_2, 1200 rpm, 2 h), (d) 1,4-NADH self-decay ($[1,4\text{-NADH}]_0$ = 6mM in 0.1 M D_2O phosphate buffer pH 7 at 20 °C) and (e) NAD^+ Borohydride Reduction Products ($[NAD^+]_0$ = 15 mM in 0.1 M D_2O phosphate buffer pH 7 at 20 °C with $[NaBH_4]_0$ = 75 mM).

Supporting Information

NADH Regeneration: A Case Study of Pt-catalyzed NAD^+ Reduction with H_2

Tony Saba,[a,#] Jianwei Li,[a,b,#] Joseph W.H. Burnett,[a] Russell F. Howe,[c] Panagiotis N. Kechagiopoulos,[a] and Xiaodong Wang[a,b,*]

[a]Chemical and Materials Engineering, School of Engineering, University of Aberdeen, Aberdeen AB24 3UE, Scotland, United Kingdom

[b]Chemical Engineering, Department of Engineering, Lancaster University, Lancaster LA1 4YW, United Kingdom

[c]Chemistry Department, University of Aberdeen, Aberdeen AB24 3UE, United Kingdom

*Corresponding Author E-mail:

xiaodong.wang@lancaster.ac.uk

[#]These authors contributed equally

1 Experimental

1.1 Materials

β-Nicotinamide adenine dinucleotide hydrate (NAD^+, ≥ 96.5%), β-nicotinamide adenine dinucleotide reduced disodium salt hydrate (NADH, ≥ 94%), potassium phosphate monobasic (KH_2PO_4, ≥ 99%), potassium phosphate dibasic trihydrate ($K_2HPO_4 \cdot 3H_2O$, ≥ 99%), sodium nitrate ($NaNO_3$, ≥ 99%), sodium hydroxide pellets (NaOH, ≥ 97%), deuterium oxide (99.9 atom % D), platinum on activated carbon (1% w/w loading), hexachloroplatinic acid solution (H_2PtCl_6, 8% w/w in water), urea (NH_2CONH_2, ≥ 99.5%), silicon dioxide (SiO_2, 99.5%) and magnesium oxide (MgO, 99.5%) were obtained from Sigma-Aldrich. Nitric acid (HNO_3, 68% d=1.42) was obtained from Fisher Scientific. EnzyChrom™ NAD/NADH assay kit was purchased from Universal Biologicals. All the chemicals were used as received without further purification. The H_2, N_2 and O_2 gases of ultrahigh purity (≥ 99.99%) were supplied by BOC.

1.2 Catalyst preparation and characterization

Pt/SiO_2 (1% w/w) was prepared through conventional impregnation method. Hexachloroplatinic acid solution (1.25 mL) was added to 50 mL of distilled water under 300 rpm stirring. SiO_2 support (4.95 g) was poured gradually to the liquid medium until the formation of a homogeneous colloidal mixture. The system was heated up to 80 °C until the water was evaporated. The resulting slurry was then further dried overnight in a static air furnace at 105 °C. The as prepared catalyst was ground and then reduced in 5% v/v H_2/N_2 (total flow of 40 mL min^{-1}) at 400 °C (5 °C min^{-1}) holding for 1 h. Upon cooling to ambient temperature, the reduced catalyst was passivated in 1% v/v O_2/He for offline characterisation and catalysis. Pt/MgO (1.5% w/w) was prepared by deposition-precipitation method following the procedure reported previously.[1] The prepared Pt/MgO was reduced in 5% v/v H_2/N_2 (total flow of 40 mL min^{-1}) at 450 °C (5 °C min^{-1}) holding for 1

h and then passivated as described above. The commercial Pt/C was used as supplied without any pre-treatment.

The Inductively-Coupled-Plasma Optical Emission Spectroscopy (ICP-OES, Vista-MPX) was employed to determine the Pt loadings. Before the tests, the samples were dissolved in either HF or a 1 : 1.2 : 7.2 mixture of HF: HNO_3 (65 %): HCl (35 %) solution by using the microwave reaction system (Anton Paar, Multiwave 3000). Temperature programmed reduction (TPR) experiments were conducted in a TPDRO 1100 (CE instruments) with a TCD detector using 5% v/v H_2/N_2. Profiles were collected for a temperature up to 500 °C at 5 °C min^{-1}. Nitrogen adsorption-desorption isotherms were obtained using a commercial automated Micromeritics Tristar II 3000 Analyser. Specific surface area was obtained from the adsorption isotherms using the standard BET method. Pore volume and pore size were determined by BJH analysis of desorption profiles. Transmission electron microscopy (TEM) images were taken on FEI Tecnai G2 F20 equipment. Particle size distribution was determined from TEM images by counting up to 400 particles. X-ray diffraction (XRD) experiments were performed on a Panalytical powder X-ray diffractometer. The diffraction patterns were recorded over an angular range of $10° < 2\theta < 90°$ with a step-size of 0.02°. By comparing the XRD patterns to the ICDD files, the crystalline phases were identified. The pZC of each catalyst was determined using the pH drift method.[2] Sodium nitrate solution ($NaNO_3$, 25 mL of 0.1 M) were added to an Erlenmeyer sitting on a shaker incubator. The pH of the solution was adjusted between 2 and 12 by adding either 0.1 M nitric acid (HNO_3) or 0.1 M sodium hydroxide (NaOH). Upon reaching the desired pH, catalyst (0.2 g) was added to the solution. 24 hours were allowed for the pH to stabilize and the final pH was recorded. The difference between the final and initial pH values ($\Delta pH = pH_{final}\text{-}pH_{initial}$) was then plotted against the initial pH, and the intersection between the curve and the line $\Delta pH = 0$ refers to the pZC of the catalyst.

1.3 Catalysis procedure

The hydrogenation of NAD^+ for NADH regeneration was conducted in a pressurized batch PARR reactor. The catalyst (5 to 20 mg) and 50 mL 0.1 M phosphate buffer solution (pH 7 and 10) containing NAD^+ (1.5 to 6 mM) were used. The system was flushed (three times) with N_2 (3 atm) and the temperature (37 °C) allowed to stabilise. Hydrogen gas was then introduced, the system was pressurised (10 atm) and stirring (at 1200 rpm considered as optimum stirring rate to avoid mass transfer limitations) engaged (time t = 0 for reaction). A non-invasive liquid sampling system via syringe (and filter) allowed the controlled removal of aliquots from the reactor.

In a series of blank tests, starting with NAD^+ solution and H_2 alone in the empty reactor or over the support alone, i.e. in the absence of Pt, did not result in any detectable conversion. Repeated reactions (shown by error bars) with different samples from the same batch of catalyst delivered raw data that were reproducible to within 10%. The activity of the catalysts was assessed using turnover frequency (TOF), calculated based on the amount of NAD^+ converted in the initial 6 min of the reaction (see **Eq. (1)**):

$$\text{TOF}\left(h^{-1}\right)=\frac{\text{moles of converted NAD}^+}{\text{moles of active Pt}}\times\frac{1}{\text{time (h)}} \quad \textbf{(1)}$$

where the moles of active Pt were calculated by the dispersion (determined from the TEM analysis). The amount of NAD^+ converted (i.e. NAD^+ conversion defined by X, see **Eq. (2)**) and selectivity towards each product (i.e. 1,4-NADH and 1,6-NADH, see **Eq. (3)**) were determined using the method developed in our previous work (i.e. by using combined enzymatic assays and UV-vis spectroscopy).[3] Selectivity of the unknown (covering all potential by-products) was calculated by closing the mass balance.

$$X_{NAD^+}(\%)=\frac{\text{Concentration}_{NAD^+,\text{initial}}(\text{mM}) - \text{Concentration}_{NAD^+,\text{left}}(\text{mM})}{\text{Concentration}_{NAD^+,\text{initial}}(\text{mM})}\times 100 \quad \textbf{(2)}$$

$$\text{Selectivity}_{\text{Compound, i}}(\%) = \frac{\text{Concentration}_{\text{Compound,i}}\,(\text{mM})}{\text{Concentration}_{\text{Reacted,NAD}^+}\,(\text{mM})} \times 100 \quad \textbf{(3)}$$

The supported Pt catalysed hydrogenation of NAD^+ was also repeated using D_2O phosphate buffer solution as solvent and a molecular analysis of the products was conducted via ^{1}H-NMR spectroscopy to understand the origin of by-products formed in the reaction. The results were compared with those of the commercial 1,4-NADH and NAD^+, a mixture of 1,2-, 1,4- and 1,6-NADH isomers prepared by sodium borohydride NAD^+ reduction and a 1,4-NADH sample left to decay for 20 h under ambient conditions. All the analyses were conducted on an Advance III HD 400 NMR from Bruker Daltonics (equipped with shielded z-gradient coils for gradient spectroscopy (GRASP)) at room temperature and reported in ppm with respect to deuterium oxide (D_2O) as internal standard.

2 Results and discussion

2.1 Characterization measurements

Figure S1 shows the characterization results for the Pt/SiO_2 catalyst. The TPR profile of Pt/SiO_2 shows two main reduction peaks (**Figure S1(a)**). The first peak is centred at 160 °C with a shoulder at around 205 °C, characteristic of the reduction of Pt(IV) of the precursor[4] and Pt(IV) in the PtO_2 phase that is formed during the drying process.[5] The second peak is a single peak centred at 395 °C attributed to the reduction of Pt(II) of the PtO_xCl_y species as reported in the literature.[5,6] A reduction temperature of 400 °C was thus selected to treat the catalyst prior to reactions. The isothermal nitrogen sorption analysis was used to determine the porous features of the catalyst and the results are shown in **Figure S1(b)**. The data show type IV isotherms with a H1 hysteresis loop characteristic of mesoporous materials according to the IUPAC standards. This is also demonstrated by the pore size distribution (see **Figure S1(c)**) that shows a broad peak between 2 and 100 nm with a mean pore size of 25.4 nm. The BET surface area of Pt/SiO_2 was evaluated to be 165 $m^2\,g^{-1}$. These results

are consistent with the literature.[7] **Figure S1(d)** shows the diffractogram of the silica support and reduced Pt/SiO_2. The broad peak between 15 and 35° is attributed to the amorphous silica. The diffraction peaks of Pt are observed in the reduced catalyst corresponding to the (111), (200), (220) and (311) planes of the metallic Pt particles (ICDD 00-004-0802). **Figure S1(e)** shows a representative TEM image of the reduced catalyst where spherical Pt particles are well dispersed with a mean particle size of 2.2 nm and narrow size distribution as given in **Figure S1(f)**.

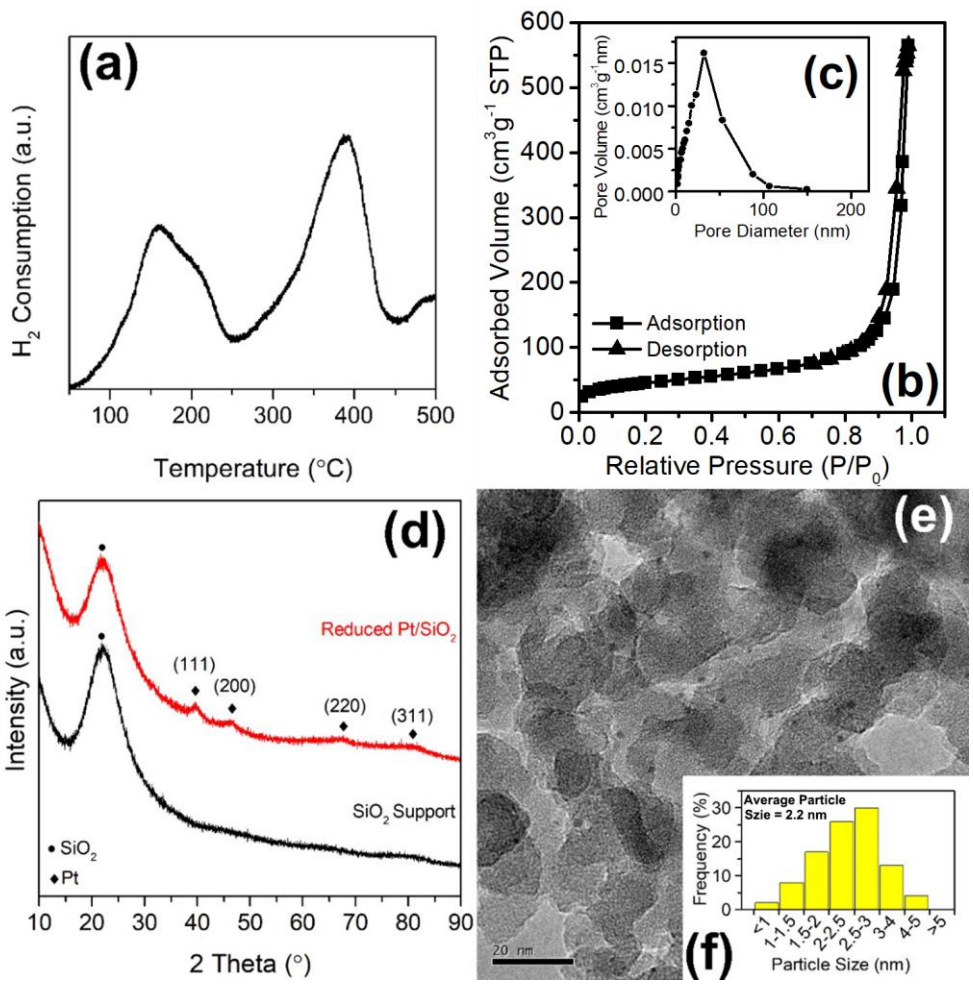

Figure S1. TPR profile of the as prepared Pt/SiO_2 catalyst (a), Isothermal N_2 adsorption-desorption curves (b) and pore size distribution (c), XRD patterns of the SiO_2 support and reduced Pt/SiO_2 (d), and representative TEM image of the reduced Pt/SiO_2 (e) with the associated particle size distribution (f).

Figure S2(a) shows the TPR profile of the as prepared Pt/MgO catalyst, which exhibits three peaks centred at 200, 360 and 440 °C. The first one and the shoulder at around 210 °C are similar to what was seen before in the Pt/SiO_2 catalyst and are attributed to the reduction of Pt(IV) species of the Pt precursor. The peaks at 360 and 440 °C can be attributed to the reduction of Pt(II) species, interacting with the support.[8] The nitrogen isotherms of the reduced Pt/MgO in **Figure S2(b)** are of type IV with a H1 hysteresis loop. The pore volume of the catalyst determined by BJH desorption method is 0.7 $cm^3\ g^{-1}$ which explains why no nitrogen filling occurred at a low relative partial pressure. The pore size distribution (**Figure S2(c)**) clearly shows a mesoporous type material with an average pore size of 28.3 nm. The BET surface area of the catalyst was determined to be 86 $m^2\ g^{-1}$. As can be seen in **Figure S2(d)**, the MgO support shows a highly crystalline periclase-like structure (2θ = 36.9, 42.9, 62.3, 74.7 and 78.6°, ICDD 01-087-0653). A broad and weak peak of Pt was discernible in the XRD pattern of the reduced catalyst due to the formation of relatively small and well dispersed Pt particles on the support. The representative TEM image (**Figure S2(e)**) of the reduced Pt/MgO shows spherical particles of Pt with an average particle size of 2.4 nm (see **Figure S2(f)**). Further representative TEM images of all catalysts employed in this work are provided in **Figure S3**.

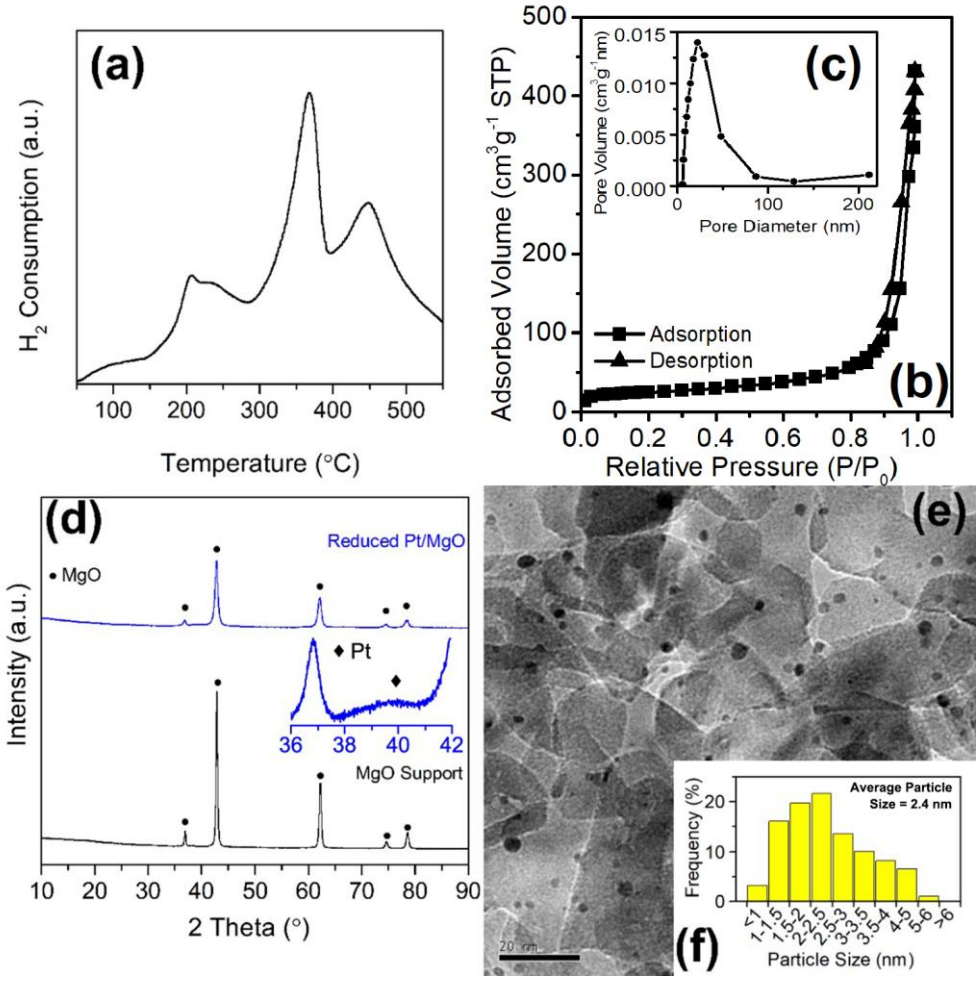

Figure S2. TPR profile of the as prepared Pt/MgO catalyst (a), Isothermal N_2 adsorption-desorption curves (b) and pore size distribution (c) of the reduced Pt/MgO, XRD patterns of the MgO support and reduced Pt/MgO (d, inset: enlarged scale of 36-42°), and representative TEM image of the reduced Pt/MgO (e) with the associated particle size distribution (f).

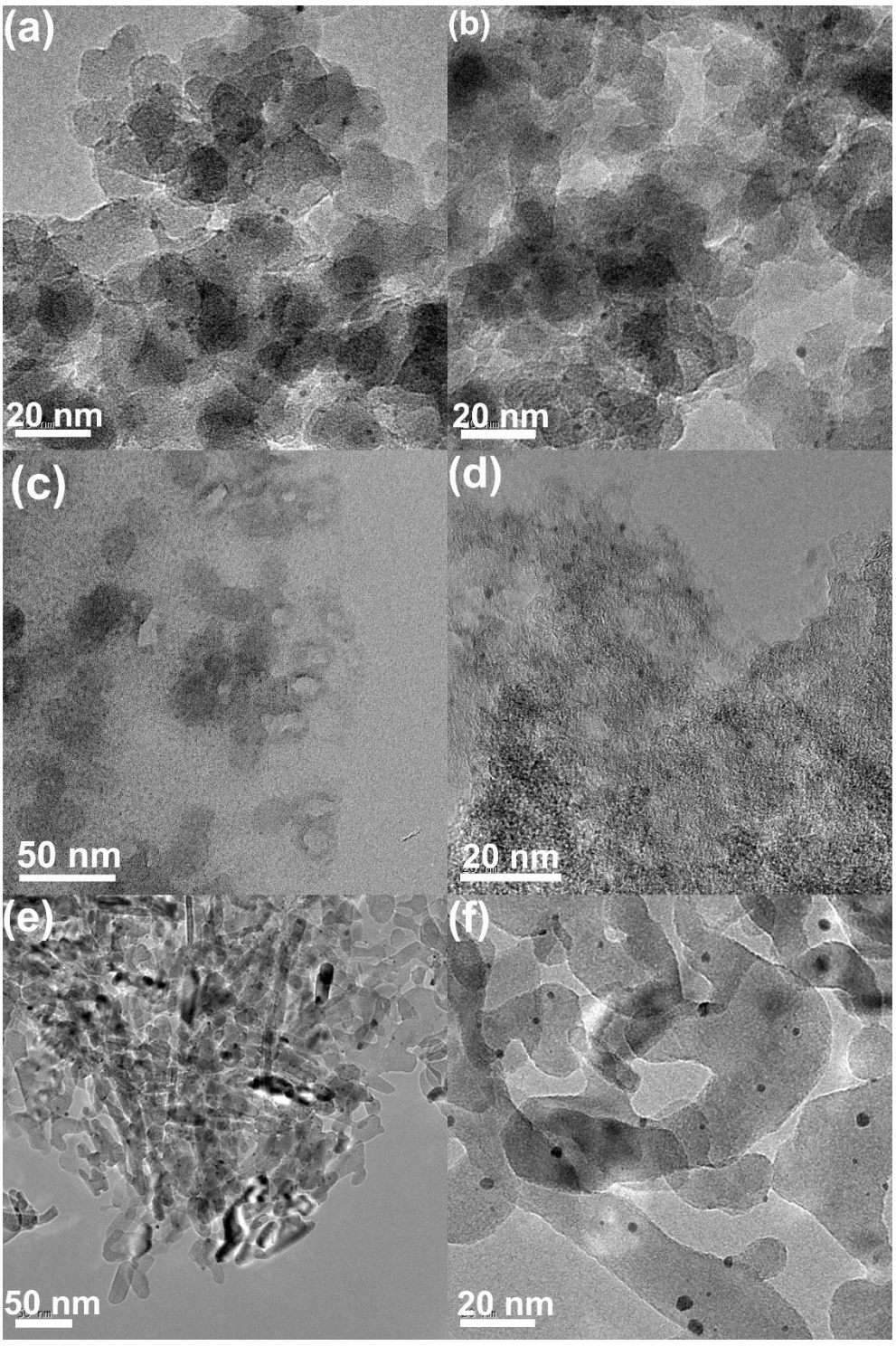

Figure S3. Representative TEM images of Pt/SiO_2 (a,b), Pt/C (c,d) and Pt/MgO (e,f) catalysts.

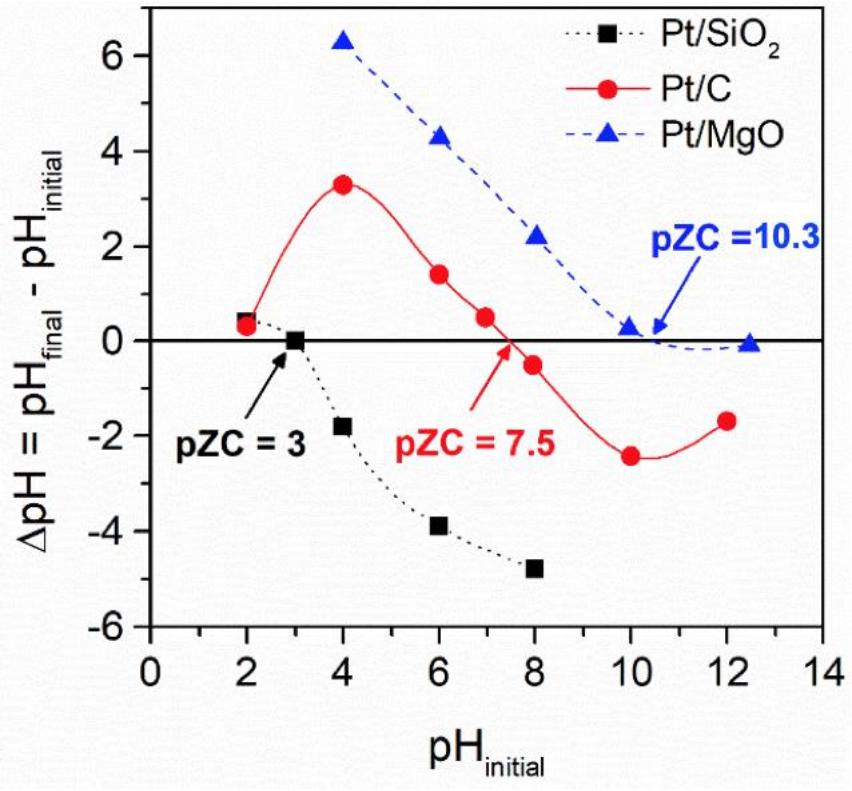

Figure S4. pH Drift Method results in the determination of the point of zero charge (pZC) of Pt/SiO_2, Pt/C and Pt/MgO catalysts.

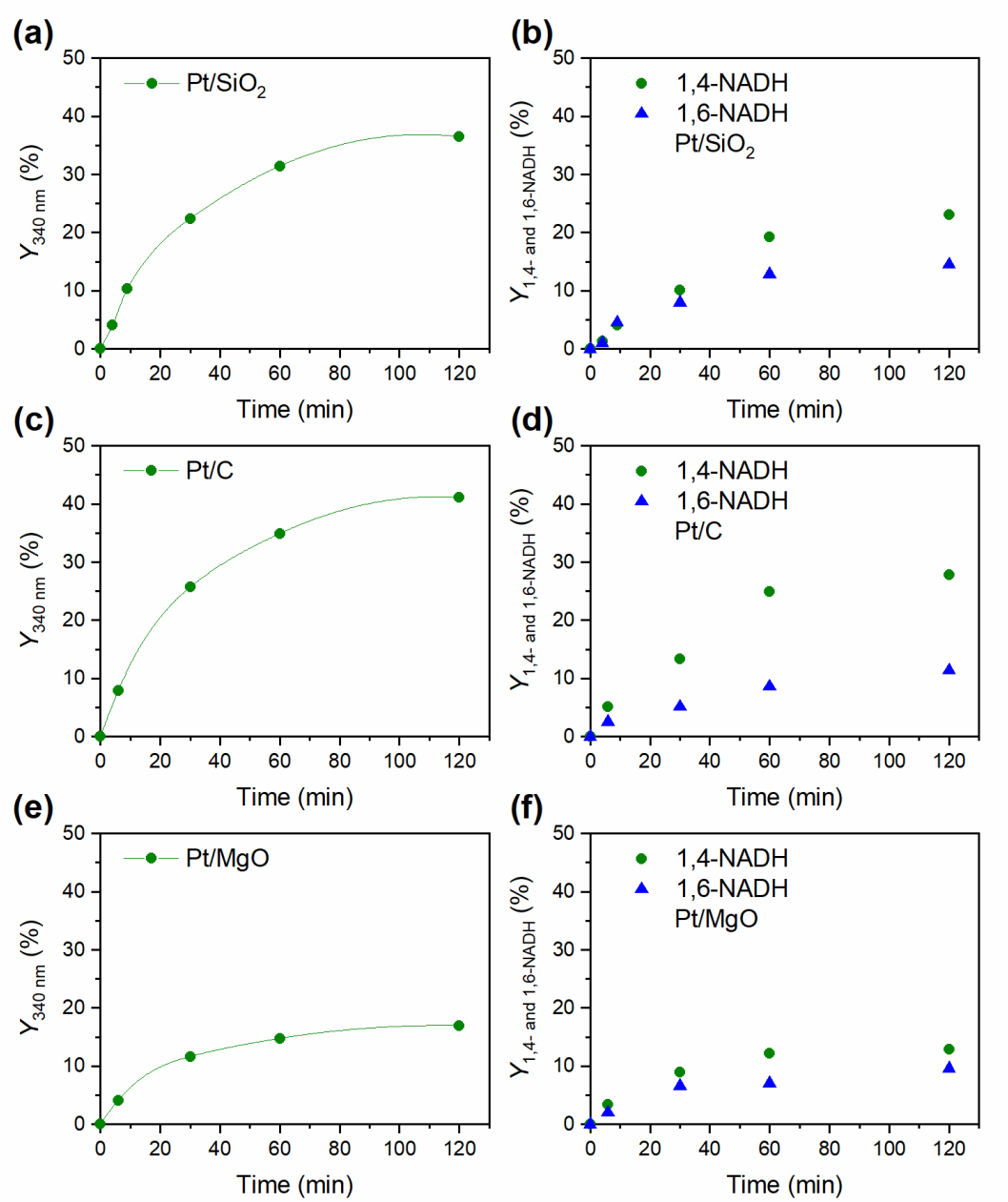

Figure S5. Yield of all products with 340 nm absorbance (a,c,e) and the true yields of 1,4-NADH and 1,6-NADH (b,d,f). Reaction conditions are the same as Figure 1 in the main text.

Figure S5 shows product yields of listed catalysts based on the absorption at 340 nm (a, c, e) and this work (b, d, f). Notably the former, as the most frequently used approach in existing publications, gives significantly higher values than the latter, with by-product information being dissimulated. That is due to the absorption overlap of desired 1,4-NADH with the undesired isomers (1,6-NADH in this case) at ~340 nm, resulting in an increased intensity as well as reaction yield. Hence it is important to apply a more considered analysis to distinguish the real yields of overall products.

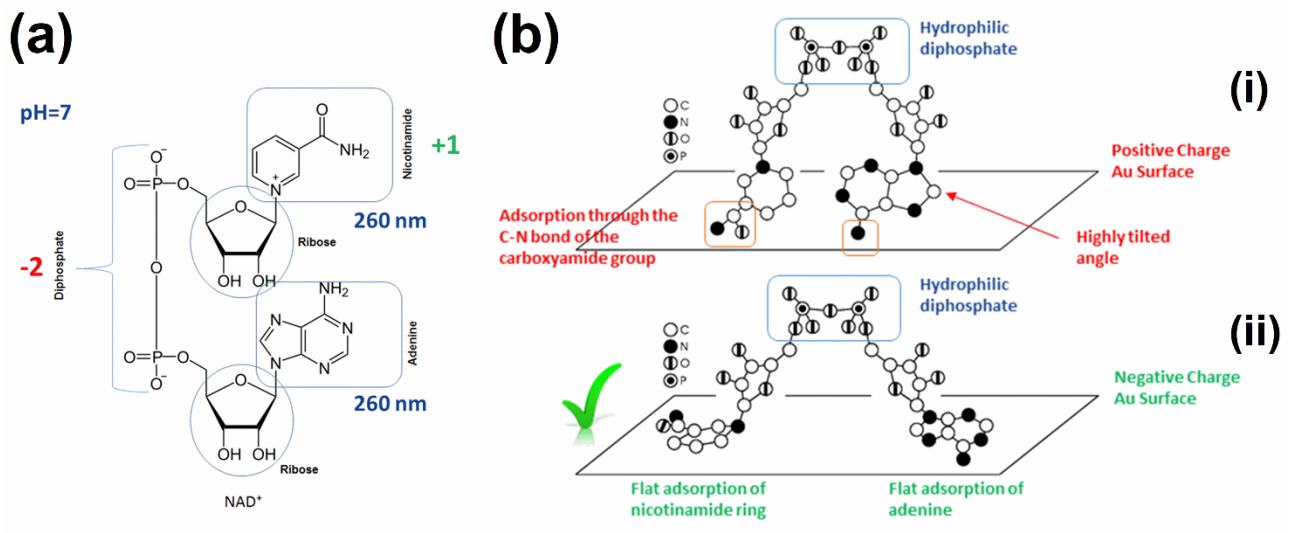

Figure S6. (a) NAD^+ structure and (b) adsorption conformations over Au surfaces. Adapted with permission from reference 9. Copyright 2007, American Chemical Society.

Damian and Omanovic have studied the interactive adsorption behaviour of NAD^+ at a gold electrode surface using polarization modulation infrared reflection absorption spectroscopy (PM-IRRAS) and attenuated total reflection Fourier transform infrared (ATR-FTIR) spectroscopy.[9] Their conclusions have shown that a negative charged surface is favourable for the nicotinamide moiety to adsorb in a flat orientation (b-ii), thus lowering the electron tunnelling distance and enabling the reduction of the molecule.(illustrated in **Figure S6**). This is consistent with our results on the surface of heterogeneous Pt/SiO_2 catalyst at pH 7. Moreover, they have also concluded that the large distance between the catalyst surface and the electron acceptor site on the nicotinamide ring (b-i) affects heterogeneous electron-transfer rate (in our case hydrogenation). This also supports our results on the Pt/MgO catalyst where the nicotinamide ring is relatively far from the surface.

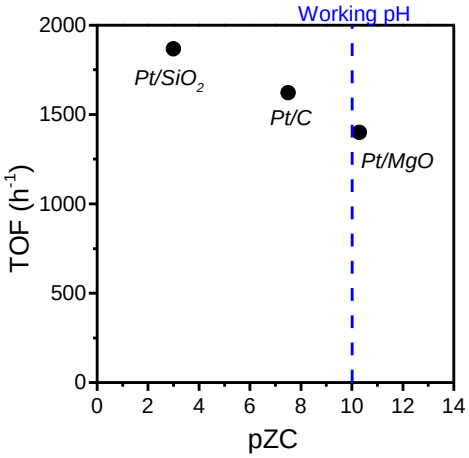

Figure S7. Effect of catalyst point of zero charge (pZC) on the initial TOF. Reaction conditions: $[NAD^+]_0$ = 1.5 mM, 5 mg catalyst, 10 atm H_2, 0.1 M phosphate buffer pH 10, 37 °C, 1200 rpm.

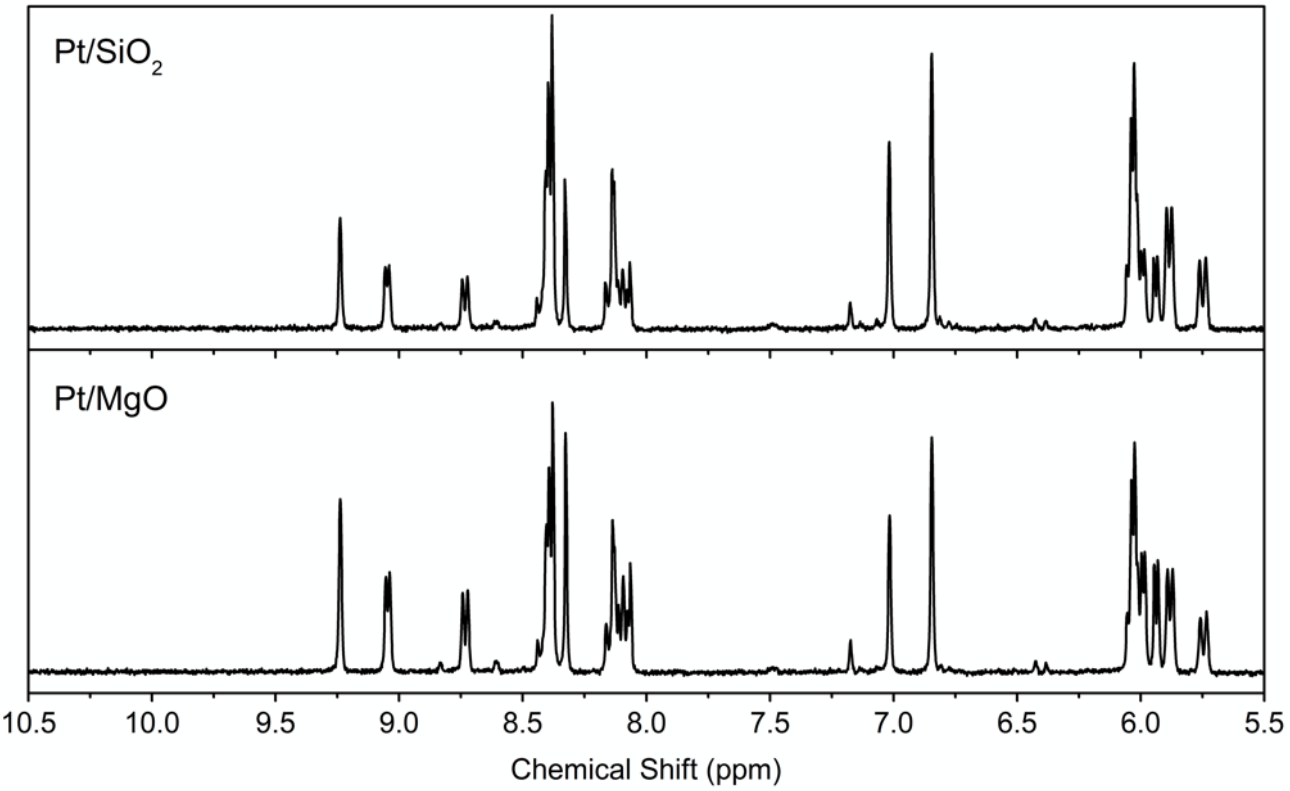

Figure S8. ^{1}H NMR spectra for Pt/SiO_2 and Pt/MgO catalyzed NADH regeneration products ($[NAD^+]_0$ = 6 mM in 0.1 M D_2O phosphate buffer pH 7, 20 mg catalyst, 37 °C, 10 atm H_2, 1200 rpm, 2 h).

3 References

(1) Saba, T.; Burnett, J. W. H.; Li, J.; Wang, X.; Anderson, J. A.; Kechagiopoulos, P. N.; Wang, X. Assessing the Environmental Performance of NADH Regeneration Methods: A Cleaner Process using Recyclable Pt/Fe_3O_4 and Hydrogen. *Catal. Today* **2020,** *339*, 281-288.

(2) Lopez-Ramon, M. V.; Stoeckli, F.; Moreno-Castilla, C.; Carrasco-Marin, F. On the Characterization of Acidic and Basic Surface Sites on Carbons by Various Techniques. *Carbon* **1999,** *37* (8), 1215-1221.

(3) Saba, T.; Burnett, J. W. H.; Li, J.; Kechagiopoulos, P. N.; Wang, X. A Facile Analytical Method for Reliable Selectivity Examination in Cofactor NADH Regeneration. *Chem. Commun.* **2020,** *56* (8), 1231-1234.

(4) Jia, J.; Shen, J.; Lin, L.; Xu, Z.; Zhang, T.; Liang, D. A Study on Reduction Behaviors of the Supported Platinum–Iron Catalysts. *J. Mol. Catal. A: Chem.* **1999,** *138* (2), 177-184.

(5) Bendahou, K.; Cherif, L.; Siffert, S.; Tidahy, H. L.; Benaïssa, H.; Aboukaïs, A. The Effect of the Use of Lanthanum-doped Mesoporous SBA-15 on the Performance of Pt/SBA-15 and Pd/SBA-15 Catalysts for Total Oxidation of Toluene. *Appl. Catal. A: Gen.* **2008,** *351* (1), 82-87.

(6) Rodríguez-Castellón, E.; Mérida-Robles, J.; Díaz, L.; Maireles-Torres, P.; Jones, D. J.; Rozière, J.; Jiménez-López, A. Hydrogenation and Ring Opening of Tetralin on Noble Metal Supported on Zirconium doped Mesoporous Silica Catalysts. *Appl. Catal. A: Gen.* **2004,** *260* (1), 9-18.

(7) Hellinger, M.; Baier, S.; Mortensen, P. M.; Kleist, W.; Jensen, A. D.; Grunwaldt, J.-D. Continuous Catalytic Hydrodeoxygenation of Guaiacol over Pt/SiO_2 and Pt/H-MFI-90. *Catalysts* **2015,** *5* (3), 1152-1166.

(8) Larimi, A. S.; Kazemeini, M.; Khorasheh, F. Highly Selective doped PtMgO Nano-sheets for Renewable Hydrogen Production from APR of Glycerol. *Int. J. Hydrogen Energy* **2016,** *41* (39), 17390-17398.

(9) Damian, A.; Omanovic, S. Interactive Adsorption Behavior of NAD^+ at a Gold Electrode Surface. *Langmuir* **2007,** *23* (6), 3162-3171.